WARSAW UNIVERSITY OF TECHNOLOGY Index 351733
FACULTY OF CIVIL ENGINEERING
COMMITTEE FOR CIVIL AND WATER ENGINEERING
POLISH ACADEMY OF SCIENCES ISSN 1230-2945

DOI: 10.24425/ace.2023.147681

ARCHIVES OF CIVIL ENGINEERING

Vol. LXIX ISSUE 4 2023

pp. 635 –661

© 2023. Wei Jing, Shuang Tian.

This is an open-access article distributed under the terms of the Creative Commons Attribution-NonCommercial-NoDerivatives License (CC BY-NC-ND 4.0, https://creativecommons.org/licenses/by-nc-nd/4.0/), which permits use, distribution, and reproduction in any medium, provided that the Article is properly cited, the use is non-commercial, and no modifications or adaptations are made.

Research paper

Seismic performance evaluation of a base-isolated steel liquid storage tank with limiting-devices considering soil-structure interaction

Wei Jing[1], Shuang Tian[2]

Abstract: Liquid storage tank is widely used in the petrochemical industry, earthquake will lead to structural damage and secondary disasters, and damping control opens up a new way for seismic design of liquid storage tank. Considering soil-structure-fluid interaction, liquid sloshing dynamic behavior and material nonlinearity, a three-dimensional calculation model of shock absorption liquid storage tank is established by combining sliding isolation and displacement-limiting devices. The dynamic responses of the liquid storage tanks under the action of Kobe and El-Centro waves are investigated, and the influence of soil-structure interaction (SSI) on the dynamic response is discussed. The results show that the damping ratio is basically between 30% and 90%. After the SSI is considered, the damping ratio of liquid sloshing wave height is increased, while the damping ratio of the dynamic response of the liquid storage tank is decreased, and the change of elastic modulus has little effect on the damping effect. The sliding isolation with displacement-limiting devices has significant damping control effects on the liquid sloshing wave height and the dynamic responses of the liquid storage tank.

Keywords: liquid storage tank, earthquake, isolation, dynamic response, shock absorption

[1] A.P., PhD., Eng., Western Engineering Research Center of Disaster Mitigation in Civil Engineering of Ministry of Education, Lanzhou University of Technology, Lanzhou 730050, China, e-mail: jingwei3276@163.com, ORCID: 0000-0002-7389-7897

[2] B.E., Eng., Western Engineering Research Center of Disaster Mitigation in Civil Engineering of Ministry of Education, Lanzhou University of Technology, Lanzhou 730050, China, e-mail: 867248803@qq.com, ORCID: 0000-0002-3597-4142

1. Introduction

There are many failure cases of liquid storage tanks under earthquakes. Generally, the seismic failure modes of liquid storage tanks mainly include liquid leakage, lifting off of the tank bottom, circumferential tension, buckling instability and fire [1–4], as shown in Figure 1. The destruction of such facilities will not only affect the normal production of enterprises, but also cause secondary disasters such as explosions and environmental pollution. Improving the seismic safety of liquid storage tanks and reducing their failure probability is of great significance for material storage, disaster prevention, emergency relief and post-disaster reconstruction.

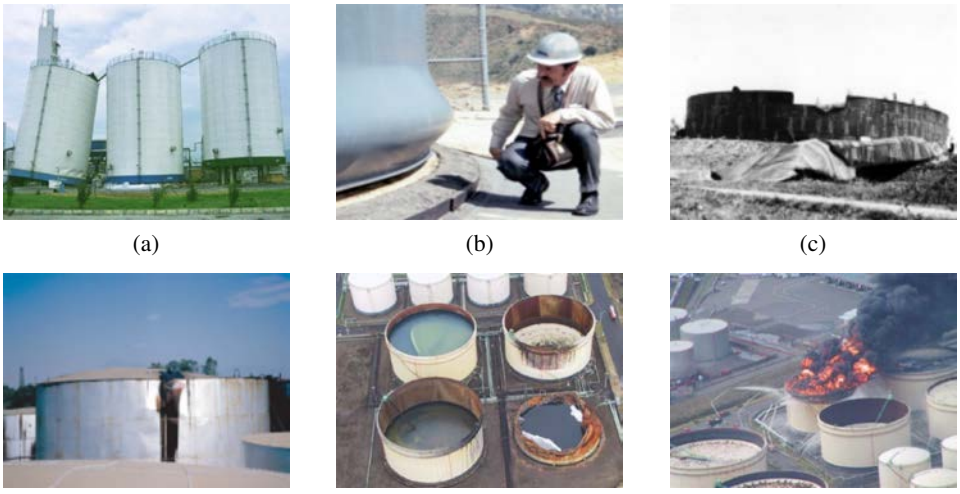

(a) (b) (c)

(d) (e) (f)

Fig. 1. Earthquake damage cases of liquid storage tank: a) support system failure, b) elephant foot flexion, c) roof failure, d) wall failure, e) liquid leakage, f) fire

With the rapid development of petrochemical industry, earthquake prevention and disaster reduction of liquid storage tank has become an important research topic, and damping control opens up a new way for seismic design of liquid storage tank. Zhang et al. [5], Yang and Gao [6], and Sun et al. [7] studied the simplified mechanical model, influence parameters, dynamic stability and dynamic response of base-isolated liquid storage tank. Safari and Tarinejad [8] studied the seismic responses of base-isolated liquid storage tank by frequency domain random method, and it is obtained that the sliding support could significantly reduce the sloshing response. Hou et al. [9] established the dynamic equation of base-isolated liquid storage structure based on Haroun Housner model. Compagnoni et al. [10] studied the seismic performance of concave sliding isolation storage tank, and found that it can reduce the base shear, but has no significant effect on the sloshing height. Cheng et al. [11] carried out the shaking table test of sliding isolation structure, and it is obtained that sliding isolation has significant control effect on structural dynamic response

and liquid sloshing. Nikoomanesh et al. [12] proposed a vertical isolation system for liquid storage tank, and the parameter research shows that the system is more effective for slender liquid storage tank. Waghmare et al. [13] studied the shock absorption effect of the semi-active control strategy using liquid viscous damper on the liquid storage tank. Kim et al. [14] established a set of optimal friction material selection system for friction pendulum isolation storage tank, and found that the lower friction coefficient is more helpful to prevent the damage of liquid storage tank by vulnerability analysis. Jiang et al. [15] proposed the optimization design method of liquid storage tank with inertial container isolation system, found that the method met the requirements of sloshing wave height and effectively reduced the base shear force and isolation layer displacement. Lv et al. [16] established a simplified mechanical model of variable curvature rolling isolated storage tank considering the liquid sloshing, it is obtained that this kind of isolation has damping effects on base shear, overturning moment and liquid sloshing. Rawat and Matsagar [17] used the shallow sphere base isolation system and floating plate to control the foundation shear and shaking response of liquid storage tank. Zhou and Zhao [18] studied the dynamic responses of anchored and replaced damper liquid storage tank through shaking table test and finite element method, and obtained that the liquid storage tank could recover its function by replacing damper after earthquake. Tsipianitis and Tsompanakis [19] used the swarm intelligence optimization algorithm to optimize the friction coefficient and radius of curvature of base-isolated liquid storage tanks with single friction pendulum and three friction pendulums. Krishnamoorthy [20] used the finite element method to simulate the friction pendulum isolation liquid storage tank, and pointed out that the finite element method considering fluid structure coupling is more suitable for analyzing FPS isolation liquid storage tank. In general, researchers have carried out a series of studies on rubber isolation, friction pendulum isolation, vertical isolation, inertial container isolation and rolling isolation liquid storage tank. Although the commonly used rubber isolation and friction pendulum isolation can reduce the dynamic responses of the liquid storage tank, it has little control effect on the sloshing wave height, and even has amplification effect. Therefore, it is still necessary to carry out effective damping control method that can reduce the dynamic responses of the liquid storage tank and the liquid sloshing wave height at the same time.

The SSI of the special site will further increase the complexity of the liquid storage tank system, which has become one of the hot issues in the study of the seismic response of liquid storage tanks. Larkin [21] proposed a frequency domain calculation method for the seismic response of liquid storage tanks in layered sites considering SSI, and obtained that the SSI had a more significant effect on liquid storage tanks on soft soils, especially slender storage tanks. Veletsos and Tang [22] considered the SSI effect by modifying the natural frequency and damping of the rigidly supported storage tank, and found that SSI could significantly reduce the impulse component of the response, but the effect on the convection component is negligible. Kianoush and Ghaemmaghami [23] used the finite element method to numerically simulate the three-dimensional soil-structure-liquid interaction of the storage tank under different earthquakes, and found that the dynamic characteristics of the liquid-tank-soil system are very sensitive to the seismic frequency

characteristics. Farajian et al. [24] used a coupled spring-damping enelemt to consider the SSI effect, and obtained that the SSI reduced the pulse displacement, overturning moment and base shear force, but had no effect on the sloshing displacement. Park et al. [25] proposed a dynamic centrifugal model test method, which accurately simulated the performance of liquid storage tanks with different base forms under earthquake action. Zhang et al. [26] studied the natural frequency of the engineering site and the influence of soil on the dynamic characteristics of the tank system, and pointed out that SSI should be considered, otherwise the vibration frequency of the tank-liquid coupling will be overestimated. Ying et al. [27] established a soil-aqueduct-fluid coupling system based on the substructure method and found that the shear wave velocity had a significant effect on the liquid sloshing. Ormeño et al. [28] conducted a shaking table test on the effect of flexible foundation on tank stress and found that compared with rigid foundation, the axial compressive stress was reduced after considering the foundation. Sun et al. [29] established a lumped parameter model to simulate the foundation and discussed the influence of soil parameters on the dynamic characteristics of the soil-tank-liquid system. Lv et al. [30] derived a simplified mechanical model considering the soil-tank-liquid interaction based on the potential flow theory and the soil model theory, obtained that the main seismic responses such as the base shear force and overturning moment of the storage tank were increased by 25%-58% after considering the soil-tank-liquid interaction. Cui et al. [31] conducted a shaking table test for liquid storage tanks, and concluded that different foundations had a greater effect on acceleration, but little effect on liquid sloshing wave height. Existing studies have shown that soil-structure interaction will affect the dynamic characteristics, pulse displacement, overturning moment, base shear and axial compressive stress of the liquid-tank-soil system, and the degree of influence depends on the type of foundation.

In summary, the dynamic behavior of the liquid storage tank is different from other types of structures, because the liquid sloshing will affect the dynamic behavior of the system, which in turn affects the damping effect of the seismic isolation liquid storage tank. The coupling effect of liquid-solid-soil under the action of earthquake will make the liquid storage tank in a more complicated stress state. Therefore, it is necessary to consider the SSI effect to carry out the seismic control research of the base-isolated storage tank. Taking the actual liquid storage tank project as the background, considering the soil-structure-fluid interaction, material nonlinearity and liquid sloshing dynamic behavior, a three-dimensional numerical calculation model of a sliding isolation storage tank with limiting devices is established. Kobe wave and El-Centro wave are selected, through comparison with non-isolated liquid storage tanks, to study the effect of sliding isolation with limiting control system on liquid storage tanks under earthquake, and the influence laws of the SSI and elastic model of the main parameters of the soil on the seismic responses are discussed.

2. Material model of the foundation

A large number of tests have shown that the Mohr–Coulomb yield criterion (Fig. 2) can reasonably describe the yield or failure behavior of soil and rock. For the foundation, the

Mohr–Coulomb criterion is used, and the corresponding equations are as follows [32–34]:

$$r' = \sqrt{\frac{S}{\pi}} = \frac{\sqrt{6}\,(6c\cos\varphi - 2I_1\sin\varphi)}{\sqrt{2\sqrt{3}\left(9 - \sin^2\varphi\right)}} \tag{2.1}$$

$$F = \frac{\sin\varphi}{3} I_1 + \left(\cos\theta + \frac{\sin\theta\sin\varphi}{\sqrt{3}}\right)\sqrt{J_2} - c\cos\varphi = 0 \tag{2.2}$$

where r' is the equivalent radius; I_1 is the stress tensor first invariant; J_2 is the second invariant of stress deviator; c is the cohesion; φ is the friction angle; θ is the lode angle, and $-30^\circ \le \theta \le 30^\circ$.

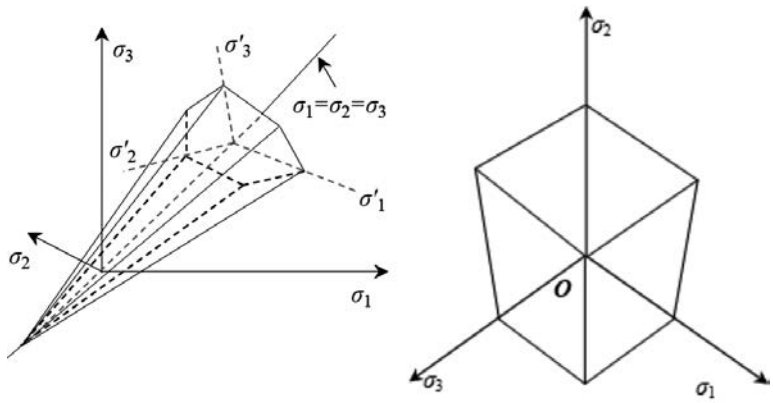

Fig. 2. Mohr–Coulomb yield criterion

The failure criterion of Mohr–Coulomb can be expressed as [35]:

$$\tau_n = c + \sigma_n \tan\varphi \tag{2.3}$$

where τ_n is the shear strength, and σ_n is the normal stress on the shear plane.

3. Contact and sliding problems

Under earthquake, the sliding isolation liquid storage tank will exist sliding and non-sliding phases, which depends on the relative size of frictional force F_f and frictional resistance F_s:

$$\begin{cases} |F_f| < F_s, & \text{non-sliding} \\ |F_f| \ge F_s, & \text{sliding} \end{cases} \tag{3.1}$$

The Coulomb friction model is used to simulate the mechanical behavior between the contact interfaces. The model defines equivalent shear stress. The surface begins to slide when the shear stress reaches this value under a certain normal compressive stress.

www.czasopisma.pan.pl PAN POLSKA AKADEMIA NAUK www.journals.pan.pl

Use the penalty function method to solve the sliding bearing contact problem, based on the traditional virtual work principle, the virtual work done by the contact force related to the virtual displacement on the contact boundary can be expressed as [36]:

$$\int_{\Omega_e} \delta u^T \rho \ddot{u}\, \mathrm{d}\Omega_e + \int_{\Omega_e} \delta u^T \xi \dot{u}\, \mathrm{d}\Omega_e + \int_{\Omega_e} \delta \varepsilon^T \sigma\, \mathrm{d}\Omega_e = \int_{\Omega_e} \delta u^T b\, \mathrm{d}\Omega_e + \int_{\Gamma_e} \delta u^T \bar{t}\, \mathrm{d}\Gamma_e + \int_{\Gamma_e} \delta g^T \bar{t}\, \mathrm{d}\Gamma_e \tag{3.2}$$

where ρ is the element's specific mass; ξ is the damping coefficient; δu is the vector containing the virtual displacement; u, $\dot{u}$ and $\ddot{u}$ are the displacement, velocity and acceleration vectors, respectively; σ is the vector of element stress tensor; $\delta\varepsilon$ is the vector of the virtual strain tensor due to δu; b is the body force vector; $\bar{t}$ is the prescribed traction vector acting on Γ_e.

4. Control equations and solutions

4.1. Liquid governing equations

At each point in the liquid domain, the velocity potential function Φ should satisfy the following condition:

$$\nabla^2 \Phi(x, y, z, t) = 0 \tag{4.1}$$

The velocity potential function on the liquid-solid coupling boundary needs to meet the following boundary condition:

$$\frac{\partial \Phi(x, y, z, t)}{\partial n} = v_n(x, y, z, t) \tag{4.2}$$

where $v_n(x, y, z, t)$ is the velocity component of the boundary along the outer normal n direction.

On the wet boundary of the liquid storage tank, the following boundary conditions exist:

$$v_n = \frac{\partial w}{\partial t} \tag{4.3}$$

The boundary condition of the free liquid surface under the action of an earthquake is:

$$\frac{1}{g}\frac{\partial^2 \Phi}{\partial t^2} + \frac{\partial \Phi}{\partial t} = 0 \tag{4.4}$$

Assuming that the liquid sloshing wave height is h, and the liquid pressure can be expressed as:

$$\frac{P}{\rho} = -gh - \frac{\partial \Phi}{\partial t} \tag{4.5}$$

www.czasopisma.pan.pl PAN POLSKA AKADEMIA NAUK www.journals.pan.pl

Based on the finite element theory, Φ can be expressed as:

$$\Phi = \sum_{i=1}^{n} N_i(x, y, z)\Phi_i(t) \tag{4.6}$$

where N_i is the shape function of the boundary element.

Replacing Eqs. (4.2), (4.3), (4.4) and (4.5), the weighted residual form of the governing equation can be expressed as [37]:

$$\begin{aligned}\int_V N_i \left[\frac{\partial}{\partial x^2} + \frac{\partial}{\partial y^2} + \frac{\partial}{\partial z^2}\right] \sum N_j \Phi_j \, \mathrm{d}V - \int_{\Gamma_1} N_i \frac{\partial}{\partial n} \sum N_j \Phi_j \, \mathrm{d}\Gamma_1 \\ + \int_{\Gamma_1} N_i v_n \, \mathrm{d}\Gamma_1 - \int_{\Gamma_2} \left[\frac{N_i}{g} \frac{\partial^2}{\partial t^2} \sum N_j \Phi_j + N_i \frac{\partial}{\partial z} \sum N_j \Phi_j\right] \mathrm{d}\Gamma_2 = 0\end{aligned} \tag{4.7}$$

The above equation is further expanded to Eq. (4.8):

$$\begin{aligned}&\int_\Gamma N_i \left[\sum \frac{\partial N_j}{\partial x} l_x \Phi_j + \sum \frac{\partial N_j}{\partial y} l_y \Phi_j + \sum \frac{\partial N_j}{\partial z} l_z \Phi_j\right] \mathrm{d}\Gamma \\ &\quad - \int_V \left[\frac{\partial N_i}{\partial x} \sum \frac{\partial N_j}{\partial x} \Phi_j + \frac{\partial N_i}{\partial y} \sum \frac{\partial N_j}{\partial y} \Phi_j + \frac{\partial N_i}{\partial z} \sum \frac{\partial N_j}{\partial z} \Phi_j\right] \\ &= \int_{\Gamma_1} N_i \sum \frac{\partial N_i}{\partial n} \Phi_j \, \mathrm{d}\Gamma_1 - \int_{\Gamma_1} N_i v_n \, \mathrm{d}\Gamma_1 + \frac{1}{g} \int_{\Gamma_2} N_i \sum N_j \frac{\partial^2 \Phi_j}{\partial t^2} \, \mathrm{d}\Gamma_2 \\ &\quad + \int_{\Gamma_2} N_i \sum N_j \frac{\partial N_j}{\partial z} \Phi_j \, \mathrm{d}\Gamma_2\end{aligned} \tag{4.8}$$

If a small slope is assumed at the interface between the liquid and the structure, the following equation can be formed:

$$\frac{\partial N_j}{\partial n} = \frac{\partial N_j}{\partial z}, \quad \text{on } \Gamma_2 \tag{4.9}$$

As a result, Eq. (4.8) can be reconverted to Eq. (4.10) [37]:

$$\begin{aligned}\int_V \left[\frac{\partial N_i}{\partial x} \sum \frac{\partial N_j}{\partial x} \Phi_j + \frac{\partial N_i}{\partial y} \sum \frac{\partial N_j}{\partial y} \Phi_j + \frac{\partial N_i}{\partial z} \sum \frac{\partial N_j}{\partial z} \Phi_j\right] \mathrm{d}V \\ + \frac{1}{g} \int_{\Gamma_2} N_i \sum N_j \frac{\partial^2 \Phi_j}{\partial t^2} \, \mathrm{d}\Gamma_2 = \int_{\Gamma_1} N_i v_n \, \mathrm{d}\Gamma_1\end{aligned} \tag{4.10}$$

Therefore, using finite element formulation of the fluid domain and using the discredited formulation of Eq. (4.1), the wave equation can be written in the following form:

$$G\ddot{P} + HP = F \tag{4.11}$$

www.czasopisma.pan.pl PAN POLSKA AKADEMIA NAUK www.journals.pan.pl

where G is the fluid mass matrices, H is the fluid stiffness; F is the force acting on the liquid domain, which depends on the boundary condition and at the interface element.

$$G_{i,j}^{e} = \sum \frac{1}{g} \int_{\Gamma^e} N_i \sum N_j \, \mathrm{d}\Gamma \tag{4.12}$$

$$H_{i,j}^{e} = \int_{V^e} \left(\frac{\partial N_i}{\partial x} \sum \frac{\partial N_j}{\partial x} + \frac{\partial N_i}{\partial y} \sum \frac{\partial N_j}{\partial y} + \frac{\partial N_i}{\partial z} \sum \frac{\partial N_j}{\partial z} \right) \tag{4.13}$$

where $G_{i,j} = \sum G_{i,j}^{e}$ and $H_{i,j} = \sum H_{i,j}^{e}$ are the constant coefficient for each element.

$$F = -\rho Q^T \left(\ddot{u}_s + \ddot{u}_g \right) \tag{4.14}$$

where Q is the coupling matrix; $\ddot{u}_s$ is the acceleration vector of the nodes at the boundary element in the structural domain; $\ddot{u}_g$ is the ground acceleration vector applied to the system.

Therefore, the dynamic equation of the interface element in the fluid domain can be expressed as [37]:

$$G\ddot{P} + C'\dot{P} + HP = -\rho_f Q^T \left(\ddot{u}_s + \ddot{u}_g \right) \tag{4.15}$$

Assuming that $F_2 = -\rho_f Q^T \ddot{u}_g$, then Eq. (4.15) is further simplified as:

$$G\ddot{P} + C'\dot{P} + HP = F_2 - \rho_f Q^T \ddot{u}_s \tag{4.16}$$

4.2. Structure control equation

The dynamic equation of the structure can be expressed as:

$$M_s \ddot{u}_s(t) + C_s \dot{u}_s(t) + K_s u_s(t) = -M_s \ddot{u}_g(t) + QP - F_f \tag{4.17}$$

where M_s, C_s and K_s are the mass, damping and stiffness, respectively; $u_s(t)$, $\dot{u}_s(t)$ and $\ddot{u}_s(t)$ are the displacement, velocity and acceleration vectors of the coupled system; $\ddot{u}_g(t)$ is the earthquake acceleration vector; Q is the fluid-structure coupling matrix; P is the hydrodynamic pressure; F_f is the friction force.

Assuming that $F_1 = -M\ddot{u}_g(t) - F_f$, then Eq. (4.17) is further simplified as:

$$M_s \ddot{u}(t) + C_s \dot{u}(t) + K_s u(t) = F_1 + QP \tag{4.18}$$

4.3. Coupling Matrix

On the liquid-solid coupling interface, the coupling matrix Q related to the liquid pressure can be expressed as:

$$QP = f \tag{4.19}$$

where P is the liquid pressure; f is the corresponding equivalent structural force.

www.czasopisma.pan.pl PAN POLSKA AKADEMIA NAUK www.journals.pan.pl

The coupling matrix can be obtained by the principle of virtual work, which can be expressed as follows [37]:

$$\int P^e u_n^e \, \mathrm{d}s = f_e^T \delta = \begin{bmatrix} f_{x1} & f_{y1} & f_{z1} & f_{x2} & f_{y2} & f_{z2} \end{bmatrix} \begin{bmatrix} u_1 & v_1 & w_1 & u_2 & v_2 & w_2 \end{bmatrix}^T \tag{4.20}$$

where P^e and u_n^e are the pressure and normal displacement along the element interface; f_e are the force acting on the element; δ is the element displacement; f_x, f_y and f_z are the node forces in x, y and z directions; u, v and w are the node displacements in the x, y, and z directions; e represents the element on the interaction boundary.

Introducing the shape function N_i at each node can connect the node displacement with the element displacement:

$$\begin{cases} u = N_1 u_1 + N_2 u_2 \\ v = N_1 v_1 + N_2 v_2 \\ w = N_1 w_1 + N_2 w_2 \end{cases} \tag{4.21}$$

The normal displacement along the interface of the coupling element is:

$$u_n = u_n + v_n + w_n = \eta N_1 u_1 + \eta N_2 u_2 + \beta N_1 v_1 + \beta N_2 v_2 + \gamma N_1 w_1 + \gamma N_2 w_2 \tag{4.22}$$

Similarly, assuming that the liquid shape function is N^f, the relationship between node pressure and element pressure can be expressed as:

$$P = \left(N^f\right)^T P^e = \begin{bmatrix} N_1^f & N_2^f \end{bmatrix} \begin{bmatrix} P_1 \\ P_2 \end{bmatrix} \tag{4.23}$$

Based on Eqs. (4.20), (4.22) and (4.23), the virtual work balance equation can be expressed as:

$$f^e = \int_{se} N_n^s N^f \, \mathrm{d}s P^e = Q^e P^e \tag{4.24}$$

where Q^e is the element coupling matrix; P^e is the element pressure; f^e is the element interface force.

4.4. Solution of liquid-solid coupling dynamic equation

Based on the above structure and liquid equations, the dynamic equation of liquid-solid coupling system in time domain can be obtained by combining Eq. (4.16) and Eq. (4.18) [37]:

$$\begin{bmatrix} M_s & 0 \\ \rho_f Q^T & G \end{bmatrix} \begin{Bmatrix} \ddot{u}_s \\ \ddot{P} \end{Bmatrix} + \begin{bmatrix} C_s & 0 \\ 0 & C' \end{bmatrix} \begin{Bmatrix} \dot{u}_s \\ \dot{P} \end{Bmatrix} + \begin{bmatrix} K_s & -Q \\ 0 & H \end{bmatrix} \begin{Bmatrix} u_s \\ P \end{Bmatrix} = \begin{Bmatrix} F_1 \\ F_2 \end{Bmatrix} \tag{4.25}$$

The above equation can be further expressed as:

$$M \begin{Bmatrix} \ddot{u}_s \\ \ddot{P} \end{Bmatrix} + C \begin{Bmatrix} \dot{u}_s \\ \dot{P} \end{Bmatrix} + K \begin{Bmatrix} u_s \\ P \end{Bmatrix} = \begin{Bmatrix} F_1 \\ F_2 \end{Bmatrix} \tag{4.26}$$

www.czasopisma.pan.pl PAN POLSKA AKADEMIA NAUK www.journals.pan.pl

The dynamic equation is solved by Newmark-β method:

$$\begin{Bmatrix} \dot{u}_s \\ \dot{P} \end{Bmatrix}_{t+\Delta t} = \begin{Bmatrix} \dot{u}_s \\ \dot{P} \end{Bmatrix}_t + [(1-\gamma)\Delta t] \begin{Bmatrix} \ddot{u}_s \\ \ddot{P} \end{Bmatrix}_t + (\gamma \Delta t) \begin{Bmatrix} \ddot{u}_s \\ \ddot{P} \end{Bmatrix}_{t+\Delta t} \tag{4.27}$$

$$\begin{Bmatrix} u_s \\ P \end{Bmatrix}_{t+\Delta t} = \begin{Bmatrix} u_s \\ P \end{Bmatrix}_t + \Delta t \begin{Bmatrix} \dot{u}_s \\ \dot{P} \end{Bmatrix}_t + \left[(0.5-\beta)\Delta t^2\right] \begin{Bmatrix} \ddot{u}_s \\ \ddot{P} \end{Bmatrix}_t + \left(\beta \Delta t^2\right) \begin{Bmatrix} \ddot{u}_s \\ \ddot{P} \end{Bmatrix}_{t+\Delta t} \tag{4.28}$$

The differential equation at time $t + \Delta t$ can be expressed as:

$$M \begin{Bmatrix} \ddot{u}_s \\ \ddot{P} \end{Bmatrix}_{t+\Delta t} + C \begin{Bmatrix} \dot{u}_s \\ \dot{P} \end{Bmatrix}_{t+\Delta t} + K \begin{Bmatrix} u_s \\ P \end{Bmatrix}_{t+\Delta t} = \begin{Bmatrix} F_1 \\ F_2 \end{Bmatrix}_{t+\Delta t} \tag{4.29}$$

Incorporating Eqs. (4.27) and (4.28) into Eq. (4.29):

$$\overline{K} \begin{Bmatrix} u_s \\ P \end{Bmatrix}_{t+\Delta t} = \begin{Bmatrix} \bar{F}_1 \\ \bar{F}_2 \end{Bmatrix}_{t+\Delta t} \tag{4.30}$$

where

$$\overline{K} = K + \frac{1}{\beta \Delta t^2} M + \frac{\gamma}{\beta \Delta t} C$$

$$\begin{Bmatrix} \bar{F}_1 \\ \bar{F}_2 \end{Bmatrix}_{t+\Delta t} = \begin{Bmatrix} F_1 \\ F_2 \end{Bmatrix}_{t+\Delta t} + M \left(\frac{1}{\beta \Delta t^2} \begin{Bmatrix} u_s \\ P \end{Bmatrix}_t + \frac{1}{\beta \Delta t} \begin{Bmatrix} \dot{u}_s \\ \dot{P} \end{Bmatrix}_t + \left(\frac{1}{2\beta} - 1 \right) \begin{Bmatrix} \ddot{u}_s \\ \ddot{P} \end{Bmatrix}_t \right)$$
$$+ C \left(\frac{\gamma}{\beta \Delta t} \begin{Bmatrix} u_s \\ P \end{Bmatrix}_t + \left(\frac{\gamma}{\beta} - 1 \right) \begin{Bmatrix} \dot{u}_s \\ \dot{P} \end{Bmatrix}_t + \left(\frac{\gamma}{2\beta} - 1 \right) \Delta t \begin{Bmatrix} \ddot{u}_s \\ \ddot{P} \end{Bmatrix}_t \right)$$

5. Numeral calculation and analysis

5.1. Calculation model

The diameter of the liquid storage tank is 21 m, the height is 16 m, and the liquid level height is 14 m. The tank wall thickness from the bottom to the top is as follows: 0–2 m is 14 mm; 2–4 m is 12 mm; 4–6 m is 10 mm; 6–10 m is 8 mm; and 10–16 m is 6 mm. The bottom plate of the liquid storage tank is made of reinforced concrete, its thickness is 10 mm, its modulus of elasticity is 2.1×10^{11} Pa, its Poisson's ratio is 0.3, and its density is 7850 kg/m^3. The bilinear elastoplastic material model and Shell 163 element are used for liquid storage tank. The liquid density is 812 kg/m^3, the bulk modulus is 1.767×10^9 Pa, the viscosity is 0.00224, and Fluid 80 element is used to simulate the liquid. The compacted soil with a radius of 10.5 m and a depth of 16 m is directly below the tank, the rest is loess, and Mohr–Coulomb model is used for the soil. The size of the soil body is $96 \times 96 \times 96$ m, and the material parameters are shown in Table 1 [38]. When earthquake actions are large, the isolation layer displacement exceeds the limit value, which can lead to auxiliary pipeline damage and liquid leakage, therefore, a corresponding displacement-limiting study is necessary [39]. In order to control the displacement of the sliding isolation layer, a total of 8 quarter arc limiting-devices are installed in the isolation layer. The limiting-devices

are made of steel rods by cold bending. The bilinear elastoplastic model and Beam 181 elements are used for the limiting-devices, the material parameters of the limiting-devices are shown in Table 2 [39]. Sliding isolation bearings are used, and the sliding surface needs to be simulated, surface-to-surface contact is used to simulate the mechanical behavior of the sliding isolation. The parameters of the contact setting mainly include a normal contact stiffness coefficient of 1.0, a maximum permeability tolerance of 0.1 and a friction coefficient of 0.02. Considering the liquid-solid coupling, material nonlinearity and SSI effect, a three-dimensional numerical calculation model of the base-isolated liquid storage tank with limiting devices is established by using the finite element software ANSYS, as shown in Fig. 3.

Table 1. Soil material parameters

Type	Elastic Modulus (Pa)	Poisson's ratio	Density (kg/m^3)	Cohesion (kPa)	Friction angle (°)
Loess	8×10^6	0.3	1510	10	21.5
Compacted soil	14.57×10^6	0.3	1560	29	31.0

Table 2. Material parameters of limiting-devices

Elastic Modulus (Pa)	Poisson's ratio	Yield Strength (MPa)	Density (kg/m^3)	Strain hardening modulus (Pa)	Yield strain	Maximum plastic strain
2×10^{11}	0.3	235	7800	2×10^9	0.001	0.02

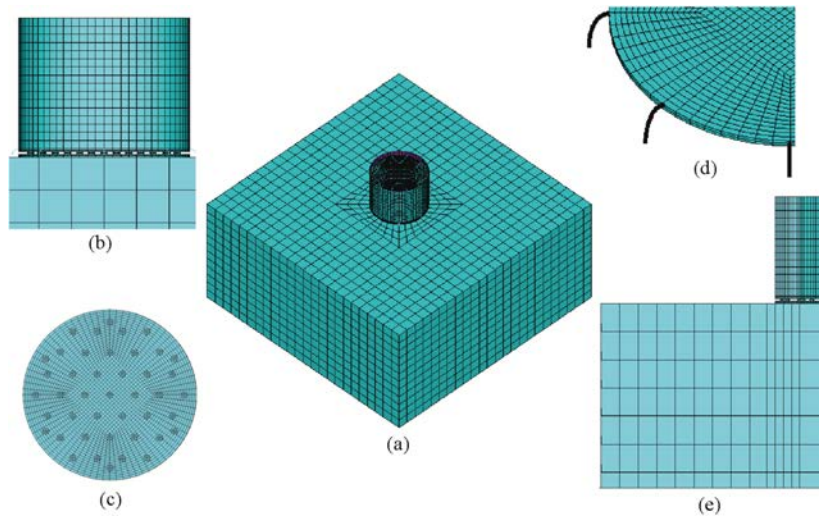

Fig. 3. Calculation model: a) overall model, b) isolation layer, (c) bearing arrangement, (d) limiting-device, (e) section view

5.2. Earthquake waves

With the help of the strong earthquake database of the Pacific Earthquake Engineering Research Center, the Kobe wave and El-Centro wave are selected as seismic inputs. The specific information of seismic waves is shown in Table 3. The time interval of Kobe wave is 0.01 s, the time interval of El-Centro wave is 0.02 s, the earthquake duration is chosen as 20s, the PGA is adjusted to 0.40 g, and the acceleration time history curves and acceleration response spectra of Kobe wave and El-Centro wave are shown in Figs. 4 and 5.

Table 3. Earthquake information

No.	Earthquake waves	Station	Duration	Predominent period (s)	PGA (g)	Year	Mechanism
1	Kobe	Kakogawa	40.90 s	0.16	0.3447	1995	Strike slip
2	El-Centro	El-Centro Array #9	53.46 s	0.56	0.3417	1940	Strike slip

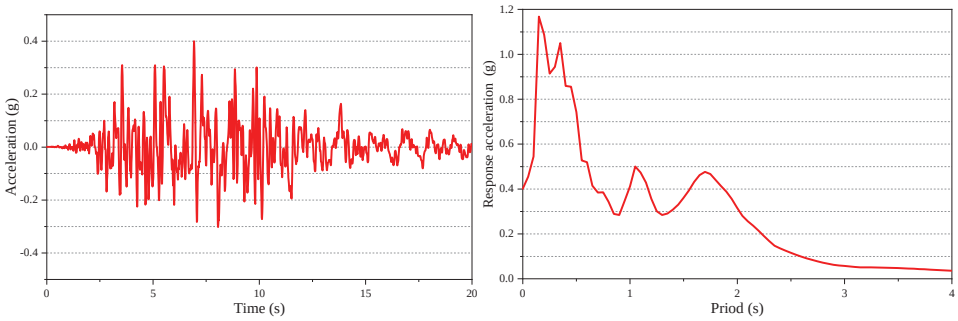

(a) (b)

Fig. 4. Kobe wave: a) acceleration, b) acceleration response spectrum

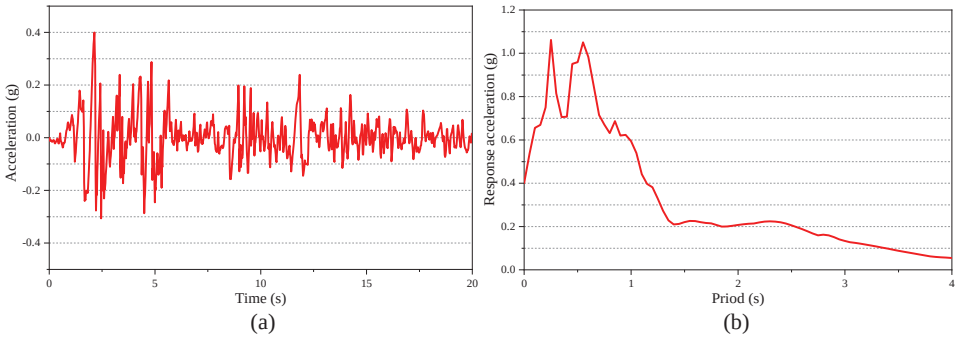

(a) (b)

Fig. 5. El-Centro wave: a) acceleration, b) acceleration response spectrum

5.3. Earthquake responses

Important dynamic responses such as liquid sloshing wave height, wall circumferential stress, wall axial stress, bottom shear force, bottom overturning moment, wall acceleration and wall equivalent stress are selected as the analysis objects, without considering SSI and considering SSI, the damping effects of the sliding isolation with limiting devices control system on the dynamic responses of the liquid storage tank are studied.

To quantitatively evaluate the effectiveness of shock absorption control, the seismic-reduction ratio R is defined:

$$R = \frac{D_{\text{No-isolation}} - D_{\text{Isolation}}}{D_{\text{No-isolation}}} \%, \tag{5.1}$$

where $D_{\text{No-isolation}}$ and $D_{\text{Isolation}}$ are the dynamic responses of the no-isolation and isolation liquid storage tanks.

5.3.1. Liquid sloshing wave height

Liquid sloshing is an important feature of liquid storage tanks under earthquake action, and the height of the liquid sloshing wave will cause damage to the top cover and cause liquid leakage, which not only wastes resources, but also causes environmental pollution and even fire. Therefore, it is necessary to control the height of the liquid sloshing wave under the action of the earthquake. Figs. 6 and 7 are the time history curves of the liquid sloshing wave height of the liquid storage tank under the action of Kobe wave and El-Centro wave.

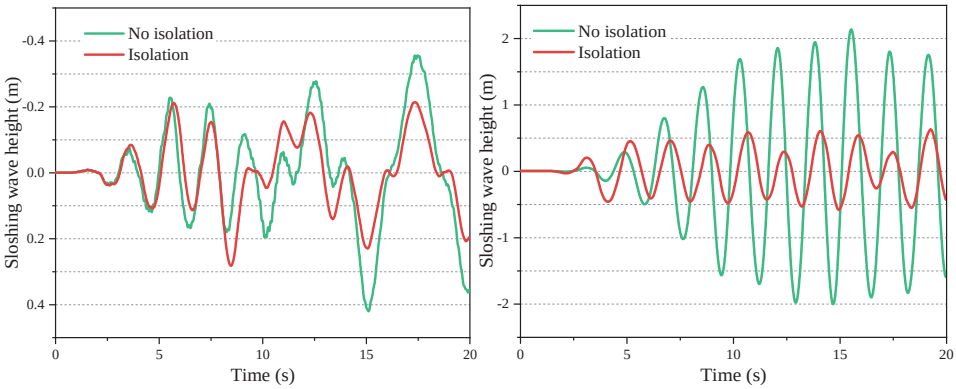

Fig. 6. Liquid sloshing wave height under Kobe wave: a) without considering SSI, b) considering SSI

As shown in Fig. 6, without considering the SSI effect, the maximum liquid sloshing wave height of the no isolation liquid storage tank is 0.42 m, and the maximum liquid sloshing wave height of the isolation liquid storage tank is 0.28 m under the Kobe earthquake, and the seismic-reduction ratio is 33.3%. After the SSI effect being considered, the liquid sloshing wave height is increased obviously, the maximum liquid sloshing wave

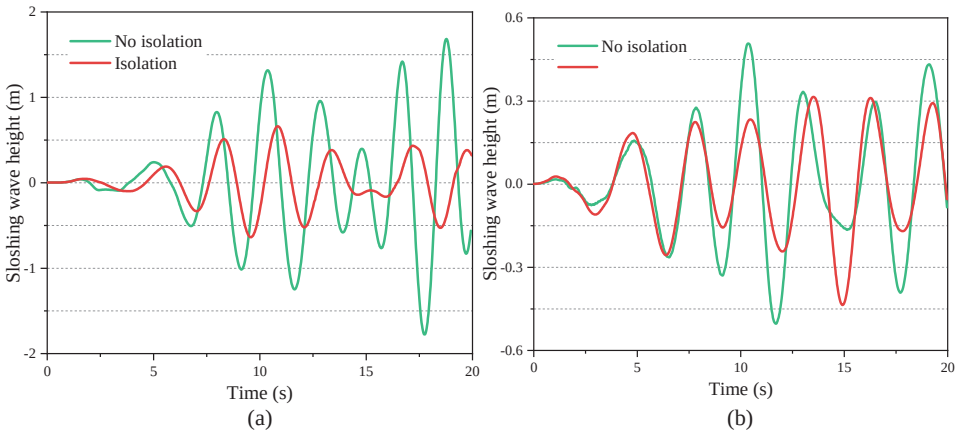

Fig. 7. Liquid sloshing wave height under El-Centro wave: a) without considering SSI, b) considering SSI

height of the no isolation liquid storage tank is 2.1 m, which exceeds the reserved freeboard height, while the maximum liquid sloshing wave height of the isolation liquid storage tank is 0.63 m under the Kobe earthquake, and the seismic-reduction ratio is 70.0%.

As shown in Fig. 7a, without considering the SSI effect, the maximum liquid sloshing wave height of the no isolation liquid storage tank is 0.50 m, and the maximum liquid sloshing wave height of the isolation liquid storage tank is 0.32 m under the El-Centro earthquake, and the seismic-reduction ratio is 36.0%. As shown in Fig. 7b, with the SSI effect being considered, the liquid sloshing wave height is increased obviously, the maximum liquid sloshing wave height of the no isolation liquid storage tank is 1.68 m, which is close to the reserved freeboard height, while the maximum liquid sloshing wave height of the isolation liquid storage tank is 0.65 m under the El-Centro earthquake, and the seismic-reduction ratio is 61.3%.

It can be seen that the sliding isolation with limiting devices control system can effectively reduce the liquid sloshing wave height. After considering the SSI effect, the liquid sloshing wave height is significantly amplified because the structure period is prolonged and close to the liquid sloshing wave height after considering the SSI effect. However, after considering the SSI effect, the control system plays a better damping effect.

5.3.2. Wall circumferential stress

The large wall circumferential stress will lead to the “elephant foot”. This failure is also one of the most common failure modes of the non-isolated liquid storage tank. Therefore, it is necessary to explore the control effect of the sliding isolation with limiting devices control system on this failure mode. Figs. 8 and 9 show the wall circumferential stress under the action of Kobe wave and El-Centro wave, respectively.

As shown in Fig. 8, under Kobe earthquake, the wall circumferential stress reaches the maximum value at 2 m, and then decreases gradually with the wall height. When the

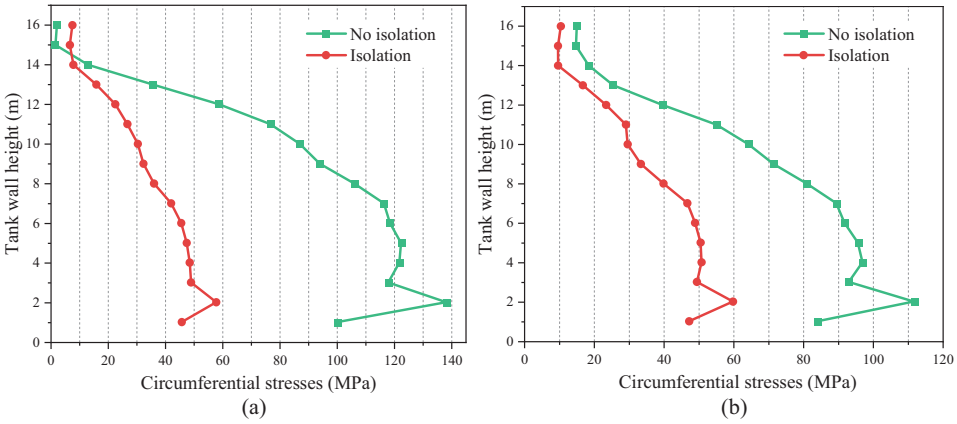

Fig. 8. Wall circumferential stress under Kobe wave: a) without considering SSI, b) considering SSI

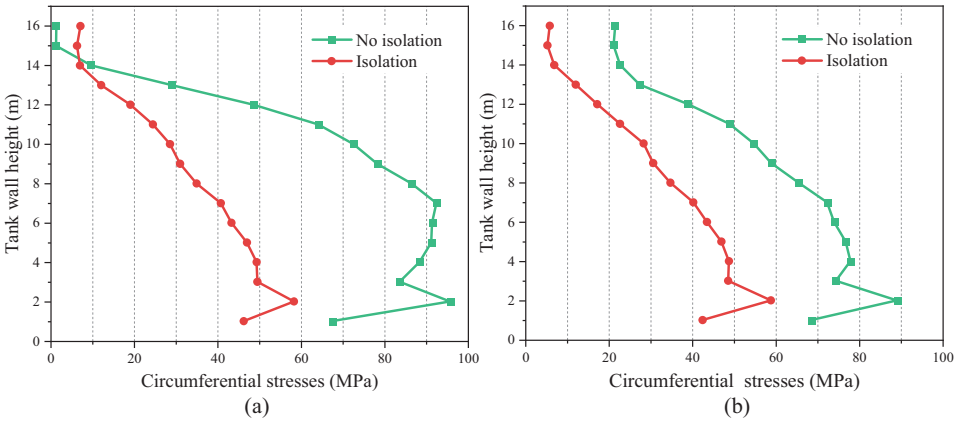

Fig. 9. Wall circumferential stress under El-Centro wave: a) without considering SSI, b) considering SSI

SSI effect is not considered, the maximum circumferential stresses of the non-isolated and isolated liquid storage tanks are 138.3 MPa and 57.8 MPa, and the seismic-reduction ratio is 58.3%. When the SSI is considered, the maximum circumferential stress of the non-isolated and isolated liquid storage tank are 111.8 MPa and 59.8 MPa, and the seismic-reduction ratio is 46.3%.

As shown in Fig. 9, under El-Centro earthquake, the wall circumferential stress reaches the maximum value at 2 m, and then decreases gradually with the wall height. When the SSI effect is not considered, the maximum circumferential stresses of the non-isolated and isolated liquid storage tanks are 95.8 MPa and 58.3 MPa, and the seismic-reduction ratio is 39.1%. When the SSI is considered, the maximum circumferential stresses of

the non-isolated and isolated liquid storage tanks are 89.1 MPa and 58.8 MPa, and the seismic-reduction ratio is 34.0%.

It can be seen that the sliding isolation limit control system has a good damping control effect on the wall circumferential stress. After considering the SSI effect, the circumferential stress of the non-isolated liquid storage tank is decreased, while the circumferential stress of the isolated liquid storage tank is increased slightly.

5.3.3. Wall axial stress

The wall axial stress is also another important reason for the "elephant foot" phenomenon of liquid storage tank. Therefore, it is also necessary to study the control effect of sliding isolation with limiting device control system on the response. Figs. 10 and 11 show the wall axial stress under the action of Kobe wave and El-Centro wave, respectively.

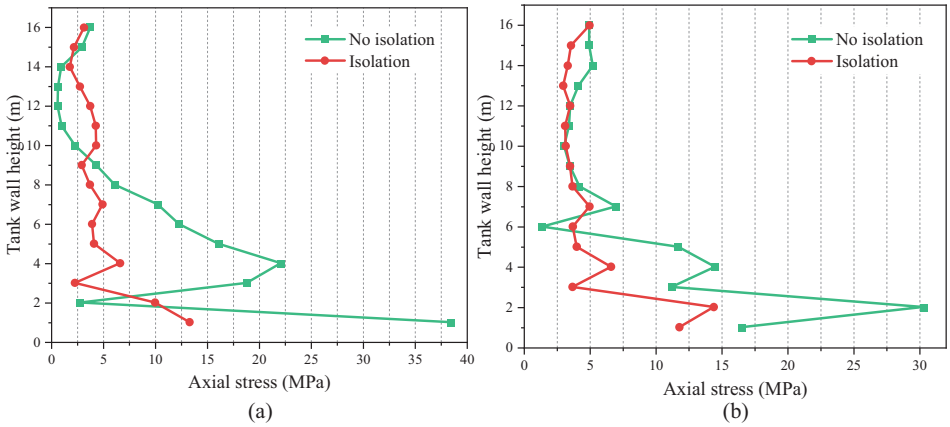

Fig. 10. Wall axial stress under Kobe wave: a) without considering SSI, b) considering SSI

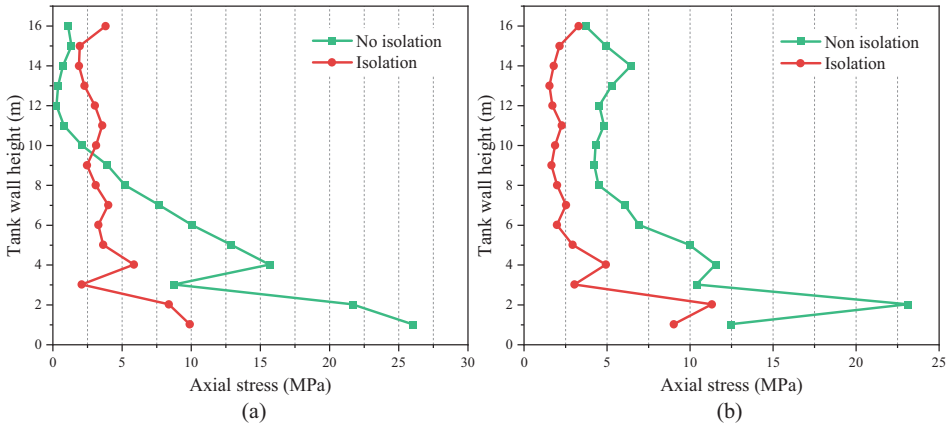

Fig. 11. Wall axial stress under El-Centro wave: a) without considering SSI, b) considering SSI

As shown in Fig. 10, under the action of Kobe earthquake, when the SSI effect is not considered, the maximum axial stress is located at 1 m, the maximum axial stresses of non-isolated and isolated liquid storage tanks are 38.4 MPa and 13.3 MPa, and the seismic-reduction ratio is 65.1%. When considering the SSI effect, the maximum axial stress is located at 2 m, the maximum axial stresses of non-isolated and isolated liquid storage tank are 30.3 MPa and 14.4 MPa, and the seismic-reduction ratio is 52.5%.

As shown in Fig. 11, under the action of El-Centro earthquake, when the SSI effect is not considered, the maximum axial stress is located at 1m, the maximum axial stresses of non-isolated and isolated liquid storage tanks are 26.0 MPa and 10.0 MPa, and the seismic-reduction ratio is 60.1%. When considering the SSI effect, the maximum axial stress is located at 2 m, the maximum axial stresses of non-isolated and isolated liquid storage tanks are 23.1 MPa and 11.3 MPa, and the seismic-reduction ratio is 51.1%.

It can be seen that the sliding isolation with limiting devices control system has a good damping control effect on the wall axial stress, and the damping effect under the action of Kobe wave is obviously better than that of El Centro wave.

5.3.4. Base shear

The base shear has an important influence on the design of the isolation layer. Figs. 12 and 13 are the time history curves of the base shear of the liquid storage tank under the action of Kobe wave and El Centro wave, respectively.

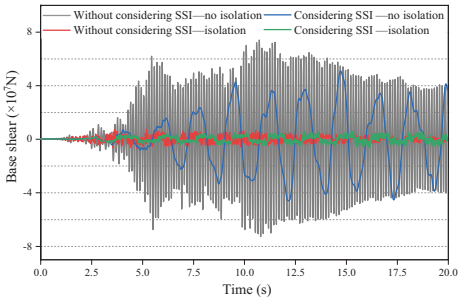

Fig. 12. Base shear under Kobe wave

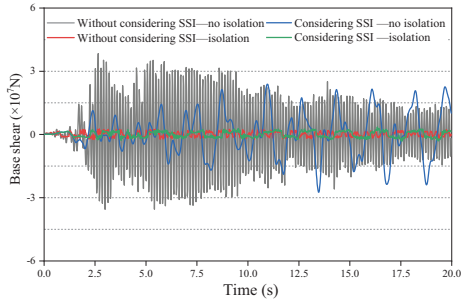

Fig. 13. Base shear under El-Centro wave

As shown in Fig. 12, under the action of Kobe earthquake, when the SSI effect is not considered, the maximum base shears of non-isolated and isolated liquid storage tanks are 74067.9 kN and 7233.1 kN, and the seismic-reduction ratio is 90.2%. After considering the SSI effect, the maximum base shears of non-isolated and isolated liquid storage tank are 51068.8 kN and 5855.4 kN, and the seismic-reduction ratio is 88.5%.

As shown in Fig. 13, under the action of El-Centro earthquake, when the SSI effect is not considered, the maximum base shears of non-isolated and isolated liquid storage tanks are 38343.7 kN and 3530.2 kN, and the seismic-reduction ratio is 90.1%. After considering the SSI effect, the maximum base shears of non-isolated and isolated liquid storage tanks are 23814.1 kN and 3508.3 kN, and the seismic-reduction ratio is 85.2%.

It can be seen that the sliding isolation limit control system has a very significant damping control effect on the base shear of the liquid storage tank. After considering the SSI effect, the base shear is decreased significantly and the damping ratio is decreased slightly.

5.3.5. Base overturning moment

Figures 14 and 15 are the time history curves of base overturning moment of liquid storage tank under the seismic action of Kobe wave and El-Centro wave, respectively.

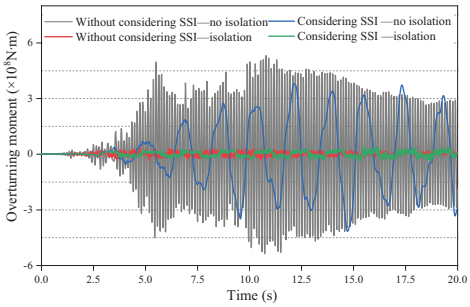

Fig. 14. Overturning moment under Kobe wave

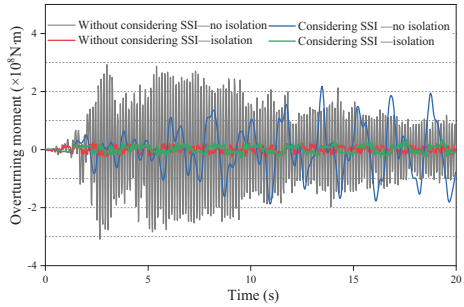

Fig. 15. Overturning moment under El-Centro wave

As shown in Fig. 14, under the action of Kobe wave earthquake, when the SSI effect is not considered, the maximum base overturning moment of non-isolated and isolated liquid storage tanks are 531401.4 kN·m and 33531.0 kN·m, and the seismic-reduction ratio is 93.2%. After considering SSI effect, the maximum base overturning moment of non-isolated and isolated liquid storage tanks are 378689.6 kN·m and 40135.3 kN·m, and the seismic-reduction ratio is 89.4%.

As shown in Fig. 15, under the action of El-Centro wave earthquake, when the SSI effect is not considered, the maximum base overturning moment of non-isolated and isolated liquid storage tanks are 292161.3 kN·m and 26102.6 kN·m, and the seismic-reduction ratio is 91.1%. After considering SSI effect, the maximum base overturning moment of non-isolated and isolated liquid storage tanks are 217614.1 kN·m and 35275.7 kN·m, and the seismic-reduction ratio is 88.8%.

It can be seen that the sliding isolation with limiting devices control system has a very significant damping control effect on the base overturning moment when considering and not considering the SSI. After considering the SSI effect, the base overturning moment is decreased significantly and the damping ratio is decreased slightly.

5.3.6. Tank acceleration

Because acceleration is often used as seismic input in time history analysis, the acceleration response of structure is often used to calculate the amplification factor, which makes the acceleration of structure become one of the important objects of earthquake response

analysis. Figs. 16 and 17 are the time history curves of tank wall acceleration under Kobe wave and El-Centro wave.

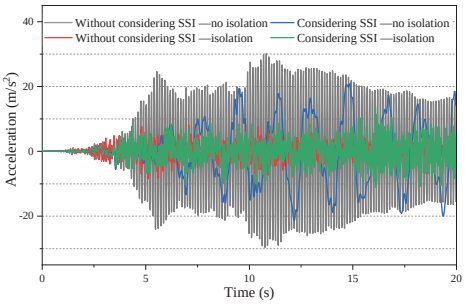

Fig. 16. Tank acceleration under Kobe wave

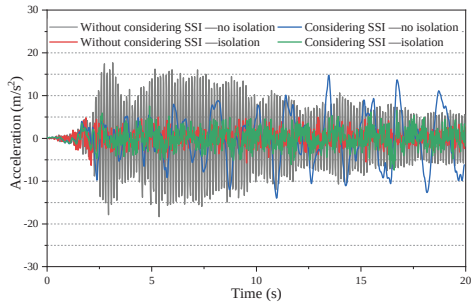

Fig. 17. Tank acceleration under El-Centro wave

As shown in Fig. 16, under the Kobe earthquake, when the SSI effect is not considered, the maximum accelerations of the non-isolated and isolated liquid storage tanks are 30.2 m/s^2 and 8.1 m/s^2, and the seismic-reduction ratio is 72.4%. After considering the SSI effect, the maximum accelerations of the non-isolated and isolated liquid storage tanks are 21.4 m/s^2 and 8.1 m/s^2, and the seismic-reduction ratio is 45.3%.

As shown in Fig. 17, under the El-Centro earthquake, when the SSI effect is not considered, the maximum accelerations of the non-isolated and isolated liquid storage tanks are 17.7 m/s^2 and 6.3 m/s^2, and the seismic-reduction ratio is 64.4%. After considering the SSI effect, the maximum accelerations of the non-isolated and isolated liquid storage tanks are 14.8 m/s^2 and 7.3 m/s^2, and the seismic-reduction ratio is 51.4%.

It can be seen that the sliding isolation with limiting devices control system has a very significant damping effect on the tank acceleration when considering and not considering the SSI. After considering the SSI effect, the tank acceleration is significantly reduced and the damping effect is slightly weakened.

The acceleration response of the tank wall is analyzed by spectrum:

$$A(\omega) = \frac{1}{2\pi} \int_{-T/2}^{T/2} A(t) e^{-i\omega t} \, \mathrm{d}t \tag{5.2}$$

where $A(t)$ is the acceleration response; $A(\omega)$ is the fourier transform of $A(t)$.

The spectrum curves are obtained by Fourier transform, as shown in Figs. 18 and 19.

It can be seen from Figs. 18 and 19 that the frequency of the liquid storage tank is significantly reduced after considering the SSI effect, mainly because the cycle of the liquid storage tank system is prolonged after considering the SSI effect.

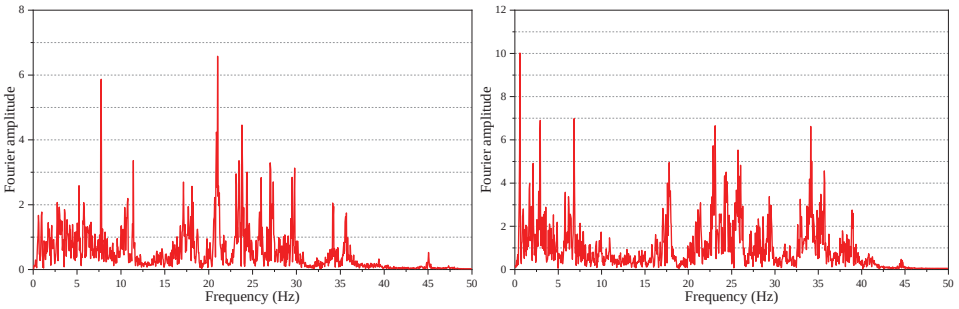

(a) (b)

Fig. 18. Spectrum curve of isolated liquid storage tank under Kobe wave:
a) without considering SSI, b) considering SSI

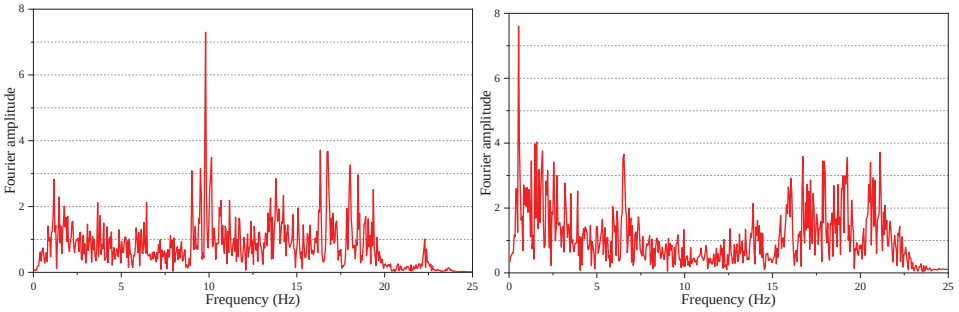

(a) (b)

Fig. 19. Spectrum curve of isolated liquid storage tank under El-Centro wave:
a) without considering SSI, b) considering SSI

5.3.7. Wall equivalent stress

Stress nephogram can intuitively show the distribution of dynamic response of liquid storage tank, which plays an important role in determining the weak parts. Equivalent stress is used to characterize the stress distribution of liquid storage tank.

Under the action of Kobe and El Centro waves, the wall equivalent stresses are shown in Figs. 20 and 21.

As shown in Fig. 20, under the action of Kobe wave, when the SSI effect is not considered, the maximum equivalent stresses of the non-isolated and isolated liquid storage tanks are is 170.0 MPa and 58.7 MPa, and the seismic-reduction ratio is 65.5%. After considering the SSI effect, the maximum equivalent stresses of the non-isolated and isolated liquid storage tanks are 126.0 MPa and 64.1 MPa, and the seismic-reduction ratio is 50.0%.

As shown in Fig. 21, under the action of El-Centro wave, when the SSI effect is not considered, the maximum equivalent stresses of the non-isolated and isolated liquid storage tanks are is 110.0 MPa and 58.2 MPa, and the seismic-reduction ratio is 47.1%. After considering the SSI effect, the maximum equivalent stresses of the non-isolated and

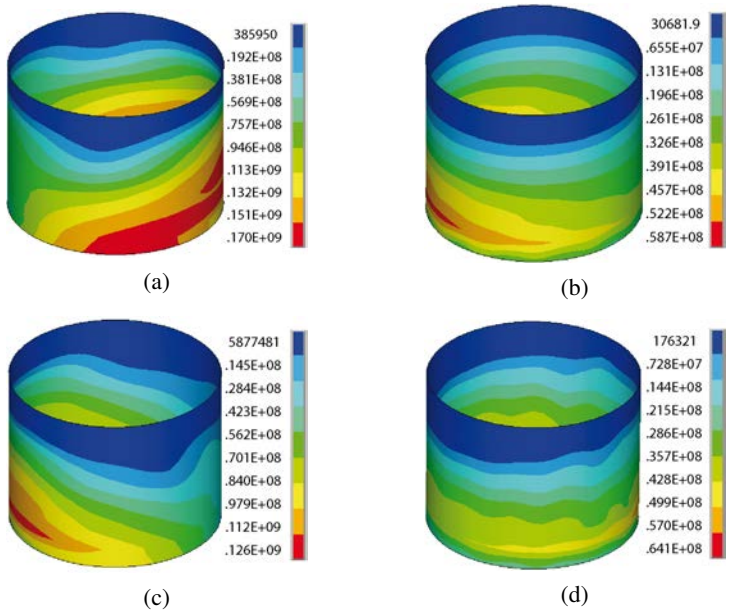

Fig. 20. Equivalent stress under the action of Kobe wave (Unit: Pa): a) without considering SSI effect-non isolation, b) without considering SSI effect-isolation, c) considering SSI effect-non isolation, d) considering SSI effect-isolation

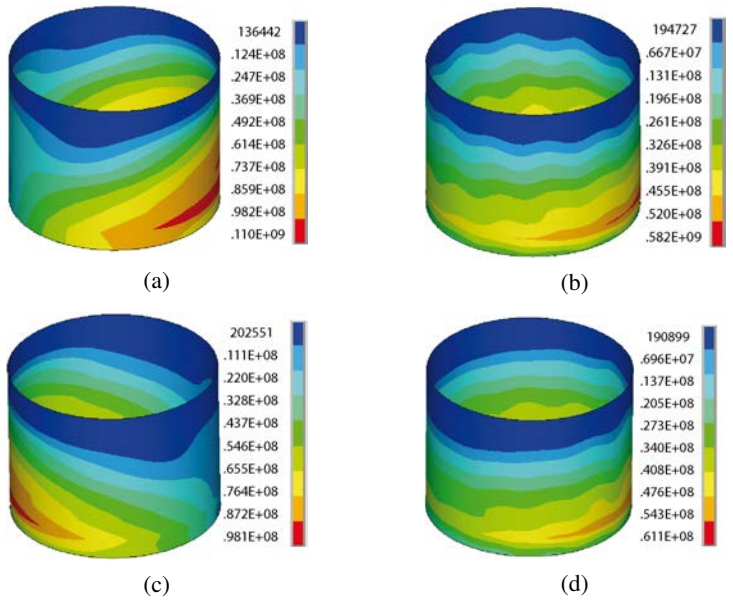

Fig. 21. Equivalent stress under the action of El-Centro wave (Unit: Pa): a) without considering SSI effect-non isolation, b) without considering SSI effect-isolation, c) considering SSI effect-non isolation, d) considering SSI effect-isolation

isolated liquid storage tanks are 98.1 MPa and 47.1 MPa, and the seismic-reduction ratio is 37.7%.

It can be seen that the sliding isolation with limiting devices control system has a significant damping effect on the tank equivalent stress. The damping effect under Kobe earthquake is better than El-Centro wave. After considering SSI effect, the damping effect is also significantly weakened.

5.4. Influence of soil elastic modulus on dynamic responses

Elastic modulus is one of the important parameters of soil, which has an important impact on foundation settlement and isolation effect, especially in soft soil site, which may make the common rubber isolation ineffective. In order to study the damping control effect of the sliding isolation with limiting devices control system on the liquid sloshing wave height and dynamic response of the liquid storage tank under different soils, three soils with different elastic modulus are selected, as shown in Table 4.

Table 4. Elastic modulus (MPa)

Elastic modulus	Soil types		
	S1	S2	S3
Values	8	16	32

5.4.1. Liquid sloshing wave height

Figure 22 is the histograms of the maximum liquid sloshing wave height of the liquid storage tank under the action of Kobe wave and El-Centro wave under different elastic modulus.

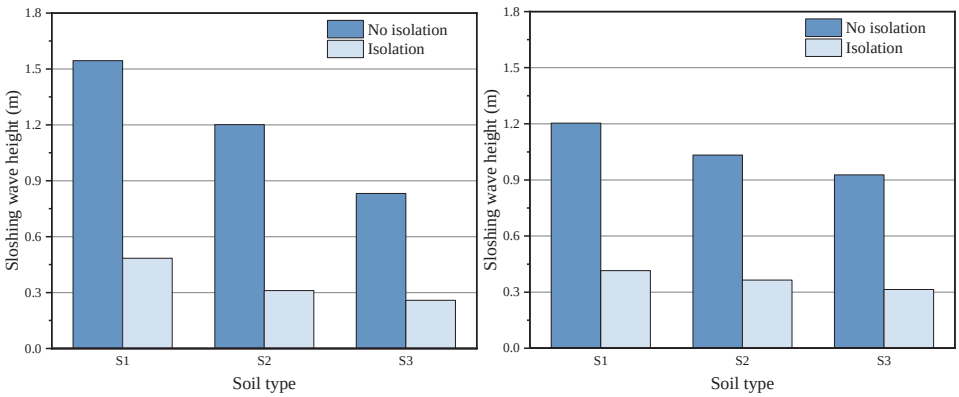

Fig. 22. Maximum liquid sloshing wave height under different soils: a) Kobe wave; b) El-Centro wave

As shown in Fig. 22, under the Kobe earthquake, the maximum liquid sloshing wave heights of the non-isolated liquid storage tank are 1.54 m, 1.20 m and 0.83 m under the soil types of S1, S2 and S3, while the maximum liquid sloshing wave heights of the isolated liquid storage tank are 0.48 m, 0.31 m and 0.26 m under the soil types of S1, S2 and S3, and the seismic-reduction ratios are 68.8%, 74.2% and 68.7% under the soil types of S1, S2 and S3. Under the El-Centro earthquake, the maximum liquid sloshing wave heights of the non-isolated liquid storage tank are 1.20 m, 1.03 m and 0.93 m under the soil types of S1, S2 and S3, while the maximum liquid sloshing wave heights of the isolated liquid storage tank are 0.41 m, 0.36 m and 0.31 m under the soil types of S1, S2 and S3, and the seismic-reduction ratios are 65.8%, 65.0% and 66.7% under the soil types of S1, S2 and S3.

In addition, under the action of Kobe earthquake, the maximum liquid sloshing wave height of non-isolated liquid storage tank under S3 soil mass is 46.1% lower than that of S1 soil mass; The maximum liquid sloshing wave height of isolation liquid storage tank under S3 soil is 45.8% lower than that of S1 soil. Under the action of El Centro earthquake, the maximum liquid sloshing wave height of non-isolated liquid storage tank under S3 soil mass is 23.0% lower than that of S1 soil mass. The maximum liquid sloshing wave height of isolation liquid storage tank under S3 soil is 32.3% lower than that of S1 soil. It can be seen that the sliding isolation limit control system has a good damping control effect on the liquid sloshing wave height of the liquid storage tank under different elastic modulus, and after considering the SSI effect, the maximum liquid sloshing wave height of the liquid storage tank decreases significantly with the increase of the elastic modulus of the soil.

It can be seen that the sliding isolation with limiting devices control system has a good damping control effect on the liquid sloshing wave height under different elastic modulus, and the maximum liquid sloshing wave height is decreased significantly with the increase of the elastic modulus of the soil.

5.4.2. Base shear

Table 5 shows the maximum base shear of liquid storage tank under the action of Kobe wave and El-Centro wave under different elastic modulus.

Table 5. Maximum base shear (kN)

Earthquakes	Model	Soil types		
		S1	S2	S3
Kobe	No isolation	56948.9	60442.3	68326.0
	Isolation	7529.3	7807.2	8325.5
El-Centro	No isolation	23482.4	31979.4	34942.5
	Isolation	2640.8	2905.7	4677.4

As shown in Table 5, under the action of Kobe earthquake, the damping ratios corresponding to the base shear of liquid storage tank are 86.8%, 87.1% and 87.8% under the soil types of S1, S2 and S3. Under the action of El-Centro earthquake, the damping ratios

corresponding to the base shear of liquid storage tank are 88.8%, 90.1% and 86.6% under the soil types of S1, S2 and S3. It can be seen that the sliding isolation with limiting devices control system has a good damping control effect on the base shear of the liquid storage tank under different elastic modulus, and the maximum base shear of the liquid storage tank is increased significantly with the increase of the elastic modulus of the soil.

5.4.3. Base overturning moment

Table 6 shows the maximum base overturning moment of the liquid storage tank under the action of Kobe wave and El-Centro wave under different elastic modulus.

Table 6. Maximum base overturning moment (kN·m)

Earthquakes	Model	Soil types		
		S1	S2	S3
Kobe	No-isolation	355721.7	423718.2	480905.9
	Isolation	35633.6	35546.2	43732.6
El-Centro	No-isolation	228405.4	250797.9	275117.1
	Isolation	28672.2	32934.8	37590.7

As shown in Table 6, under the action of Kobe earthquake, the damping ratios corresponding to the base overturning moment of liquid storage tank are 89.9%, 90.6% and 90.1% under the soil types of S1, S2 and S3. Under the action of El-Centro earthquake, the damping ratios corresponding to the Base overturning moment of liquid storage tank are 87.5%, 86.9% and 86.3% under the soil types of S1, S2 and S3. It can be seen that the sliding isolation with limiting devices control system has a good damping control effect on the base overturning moment of the liquid storage tank under different elastic modulus, and the maximum base overturning moment of the liquid storage tank is also increased significantly with the increase of the elastic modulus of the soil.

6. Conclusions

Considering the soil-structure-fluid interaction, a three-dimensional numerical calculation model of sliding isolation liquid storage tank with limiting devices is established. Through the comparison with non-isolated liquid storage tank, the damping effect of sliding isolation with limiting devices control system on the dynamic responses is studied, and the influence of SSI on seismic responses is discussed. The main conclusions are as follows:

1. When the SSI is not considered, the sliding isolation with limiting devices has a significant damping effect on the liquid sloshing wave height and the dynamic responses of the liquid storage tank.
2. After the SSI being considered, the liquid sloshing wave height of the non-isolated liquid storage tank is increased obviously, while the wall circumferential stress, wall axial stress, bottom shear force, bottom overturning moment, tank acceleration and

www.czasopisma.pan.pl PAN POLSKA AKADEMIA NAUK www.journals.pan.pl

tank equivalent stress are decreased significantly. Besides, the damping ratio of the liquid sloshing wave height is increased, while the damping ratios of the dynamic responses of the liquid storage tank are decreased after the SSI being considered.

3. After the SSI being considered, with the increase of the soil elastic modulus, the liquid sloshing wave height of the non-isolated liquid storage tank is decreased, the base shear and base overturning moment are increased, but the elastic modulus has little effect on the damping control effect.

Acknowledgements

This paper is a part of the National Natural Science Foundation of China (Grant no. 52168071, 51908267), a part of the Gansu Provincial Outstanding Youth Fund (Grant No. 23JRRA759), a part of the Scientific Research Fund of Institute of Engineering Mechanics, China Earthquake Administration (Grant No. 2020D26), and a part of the Gansu Province Higher Education Innovation Fund Project (Grant No. 2023-027).

References

[1] H. Sezen, R. Livaoglu, and A. Dogangun, "Dynamic analysis and seismic performance evaluation of above-ground liquid-containing tanks", *Engineering Structures*, vol. 30, no. 3, pp. 794–803, 2008, doi: 10.1016/j.engstruct.2007.05.002.

[2] P.K. Malhotra, T. Wenk, and M. Wieland, "Simple procedure for seismic analysis of liquid-storage tanks", *Structural Engineering International*, vol. 10, no. 3, pp. 197–201, 2000, doi: 10.2749/101686600780481509.

[3] P.K. Malhotra, "Earthquake induced sloshing in tanks with insufficient freeboard", *Structural Engineering International*, vol. 16, no. 3, pp. 222–225, 2006, doi: 10.2749/101686606778026466.

[4] K. Hatayama, "Lessons from the 2003 Tokachi-oki, Japan. Earthquake for prediction of long-period strong ground motions and sloshing damage to oil storage tanks", *Journal of Seismology*, vol. 12, no. 2, pp. 255–263, 2008, doi: 10.1007/s10950-007-9066-y.

[5] R.F. Zhang, D.G. Weng, and X.S. Ren. "Seismic analysis of a LNG storage tank isolated by a multiple friction pendulum system", *Earthquake Engineering & Engineering Vibration*, vol. 10, no. 2, pp. 253–262, 2011, doi: 10.1007/s11803-011-0063-3.

[6] H.K. Yang and B.Q. Gao, "Parametric dynamic stability analysis and vibration isolation effect assessment of base-isolated liquid storage tanks", *Journal of Vibration and Shock*, vol. 33, no. 18, pp. 96–101, 2014, doi: 10.13465/j.cnki.jvs.2014.18.016.

[7] J.G. Sun, J.F. Hao, Y. Liu, et al., "Simplified mechanical model for vibration isolation analysis of a vertical storage tank considering swinging effect", *Journal of Vibration and Shock*, vol. 35, no. 11, pp. 20–27, 2016, doi: 10.13465/j.cnki.jvs.2016.11.004.

[8] S. Safari and R. Tarinejad, "Parametric study of stochastic seismic responses of base-isolated liquid storage tanks under near-fault and far-fault ground motions", *Journal of Vibration and Control*, vol. 24, no. 24, 2018, doi: 10.1177/1077546316647576.

[9] G.L. Hou, L. Zhen, X.F. Jia, et al., "Optimal isolated models of storage tanks and its influential factors analysis", *Engineering Mechanics*, vol. 33, pp. 312–319, 2016, doi: 10.6052/j.issn.1000-4750.2015.04.S052.

[10] M.E. Compagnoni, O. Curadelli, and D. Ambrosini, "Experimental study on the seismic response of liquid storage tanks with Sliding Concave Bearings", *Journal of Loss Prevention in the Process Industries*, vol. 55, pp. 1–9, 2018, doi: 10.1016/j.jlp.2018.05.009.

[11] X.S. Cheng, W. Jing, Y.F. Du, et al., "Study on shock mitigation of concrete rectangular liquid storage structure with sliding shock insulator and limiting devices based on shaking table test", *China Civil Engineering Journal*, vol. 51, no. 12, pp. 120–132, 2018, doi: 10.15951/j.tmgcxb.2018.12.010.

[12] M.R. Nikoomanesh, M. Moeini, and M.A. Goudarzi, "An innovative isolation system for improving the seismic behaviour of liquid storage tanks", *International Journal of Pressure Vessels and Piping*, vol. 173, pp. 1–10, 2019, doi: 10.1016/j.ijpvp.2019.04.012.

[13] M.V. Waghmare, S.N. Madhekar, and V.A. Matsagar, "Semi-active fluid viscous dampers for seismic mitigation of RC elevated liquid storage tanks", *International Journal of Structural Stability and Dynamics*, vol. 19, no. 3, 2019, doi: 10.1142/S0219455419500202.

[14] J.S. Kim, J.P. Jung, J.H. Moon, et al., "Seismic fragility analysis of base-isolated LNG storage tank for selecting optimum friction material of friction pendulum system", *Journal of Earthquake and Tsunami*, vol. 13, no. 2, 2019, doi: 10.1142/S1793431119500106.

[15] Y.Y. Jiang, Z.P. Zhao, R.F. Zhang, et al., "Optimal design based on analytical solution for storage tank with inerter isolation system", *Soil Dynamics and Earthquake Engineering*, vol. 129, 2020, doi: 10.1016/j.soildyn.2019.105924.

[16] Y. Lv, Z.G. Sun, J.G. Sun, et al., "Dynamic analysis of rolling isolation with variable curvature and application in spherical tanks", *Journal of Vibration Engineering*, vol. 33, no. 1, pp. 188–195, 2020, doi: 10.16385/j.cnki.issn.1004-4523.2020.01.021.

[17] A. Rawat and V. Matsagar, "An oblate spheroid base isolator and floating surface diaphragm for seismic protection of liquid storage tank", *Journal of Earthquake Engineering*, vol. 26, no. 10, pp. 5447–5475, 2022, doi: 10.1080/13632469.2021.1875939.

[18] J.W. Zhou and M. Zhao, "Shaking table test of liquid storage tank with finite element analysis considering uplift effect", *Structural Engineering and Mechanics*, vol. 77, no. 3, pp. 369–381, 2021, doi: 10.12989/sem.2021.77.3.369.

[19] A. Tsipianitis and Y. Tsompanakis, "Optimizing the seismic response of base-isolated liquid storage tanks using swarm intelligence algorithms", *Computers & Structures*, vol. 243, 2021, doi: 10.1016/j.compstruc.2020.106407.

[20] A. Krishnamoorthy, "Finite element method of analysis for liquid storage tank isolated with friction pendulum system", *Journal of Earthquake Engineering*, vol. 25, no. 1, pp. 82–92, 2021, doi: 10.1080/13632469.2018.1498815.

[21] T. Larkin, "Seismic response of liquid storage tanks incorporating soil structure interaction", *Journal of Geotechnical and Geoenvironmental Engineering*, vol. 134, no. 12, pp. 1804–1814, 2008, doi: 10.1061/(ASCE)1090-0241(2008)134:12(1804).

[22] A.S. Veletsos and Y. Tang, "Soil-structure interaction effects for laterally excited liquid storage tanks", *Earthquake Engineering & Structural Dynamics*, vol. 19, no. 4, pp. 473–496, 1990, doi: 10.1002/eqe.4290190402.

[23] M.R. Kianoush and A.R. Ghaemmaghami, "The effect of earthquake frequency content on the seismic behavior of concrete rectangular liquid tanks using the finite element method incorporating soil-structure interaction", *Engineering Structures*, vol. 33, no. 7, pp. 2186–2200, 2011, doi: 10.1016/j.engstruct.2011.03.009.

[24] M. Farajian, M.I. Khodakarami, and D.P.N. Kontoni, "Evaluation of soil-structure interaction on the seismic response of liquid storage tanks under earthquake ground motions", *Computation*, vol. 5, no. 1, pp. 1–12, 2017, doi: 10.3390/computation5010017.

[25] H.J. Park, J.G. Ha, S.Y. Kwon, et al., "Investigation of the dynamic behaviour of a storage tank with different foundation types focusing on the soil-foundation-structure interactions using centrifuge model tests", *Earthquake Engineering & Structural Dynamics*, vol. 46, no. 14, pp. 2301–2316, 2017, doi: 10.1002/eqe.2905.

[26] R.L. Zhang, Z.W. Zhang, X.D. Cheng, et al., "Effects of soil-structure interaction on dynamic characteristics of tank-liquid systems", *Journal of Vibration and Shock*, vol. 37, no. 7, pp. 233–239, 2018, doi: 10.13465/j.cnki.jvs.2018.07.035.

[27] L. Ying, X. Meng, D. Zhou, et al., "Sloshing of fluid in a baffled rectangular aqueduct considering soil-structure interaction", *Soil Dynamics and Earthquake Engineering*, vol. 122, pp. 132–147, 2019, doi: 10.1016/j.soildyn.2019.04.008.

[28] M. Ormeño, T. Larkin, and N. Chouw, "Experimental study of the effect of a flexible base on the seismic response of a liquid storage tank", *Thin-Walled Structures*, vol. 139, pp. 334–346, 2019, doi: 10.1016/j.tws.2019.03.013.

[29] Y. Sun, D. Zhou, M. Amabili, et al., "Liquid sloshing in a rigid cylindrical tank equipped with a rigid annular baffle and on soil foundation", *International Journal of Structural Stability and Dynamics*, vol. 20, no. 3, 2020, doi: 10.1142/S0219455420500303.

[30] Y. Lv, J.G. Sun, Z.G. Sun, et al., "Simplified mechanical model for seismic design of horizontal storage tank considering soil-tank-liquid interaction", *Ocean Engineering*, vol. 198, 2020, doi: 10.1016/j.oceaneng.2020.106953.

[31] L.F. Cui, J.G. Sun, W.B. Liu, et al., "Study on sloshing effect of vertical storage tank with displacement seismic excitation", *Journal of Pressure Vessel Technology*, vol. 143, no. 2, 2021, doi: 10.1115/1.4048138.

[32] J. Shi, W. Ding, and B. Zhao, "Numerical simulation and analysis of tunnel excavation process", *Railway Engineering*, vol. 2, pp. 21–24, 2010.

[33] J.F. Labuz and A. Zang, "Mohr–Coulomb failure criterion", *Rock Mechanics and Rock Engineering*, vol. 45, pp. 975–979, 2012, doi: 10.1007/978-3-319-07713-0_19.

[34] Z.H. Lin, "Study on stress characteristics of deep roadway bolt based on nonlinear dilatancy angle model", *Archives of Civil Engineering*, vol. 68, no. 1, pp. 635–651, 2022, doi: 10.24425/ace.2022.140191.

[35] B.H.G. Brady and E.T. Brown, *Rock mechanics*. Springer, 1985.

[36] P. Wriggers, *Computational contact mechanics*. Springer, 2003.

[37] I.T. Avval, "Dynamic response of concrete rectangular liquid tanks in three-dimensional space", *Theses and dissertations*. Ryerson University, 2012.

[38] Q.B. Huang, X.N. Jia, J.B. Peng, et al., "Seismic response of loess-mudstone slope with bedding fault zone", *Soil Dynamics and Earthquake Engineering*, vol. 123, pp. 371–380, 2019, doi: 10.1016/j.soildyn.2019.05.009.

[39] X.S. Cheng, W. Jing, and L.J. Gong, "Simplified model and energy dissipation characteristics of a rectangular liquid-storage structure controlled with sliding base isolation and displacement-limiting devices", *Journal of Performance of Constructed Facilities*, vol. 31, no. 5, pp. 1–11, 2017, doi: 10.1061/(ASCE)CF.1943-5509.0001066.

Received: 2023-04-05, Revised: 2023-07-18